Status and performance of the Discovery Channel Telescope from commissioning into early science operations

William T. DeGroff, Stephen E. Levine, Thomas A. Bida, Frank Cornelius, Peter L. Collins, Edward W. Dunham, Ben Hardesty, Michael Lacasse, Mike Sweaton, Alex J. Venetiou[a], Saeid Zoonemat Kermani, Philip Massey, M. Lisa Foley, Heidi Larson, Jason Sanborn, Susan Strosahl, Ron Winner, Teznie Pugh[b]

ABSTRACT

Lowell Observatory's Discovery Channel Telescope is a 4.3m telescope designed and constructed for optical and near infrared astronomical observation. It is equipped with a cube capable of carrying five instruments and the wave front sensing and guider systems at the f/6.1 RC focus. We report on the overall operations methods for the facility, including coordination of day and night activities, and then cover pointing, and unguided and guided tracking performance of the mount. We also discuss the implementation and performance of the open loop model for, and manual wavefront sensing and correction with the active optics system. We conclude with a report on the early integrated image quality and science performance of the facility using the first science instrument, the Large Monolithic Imager.

Keywords: Discovery Channel Telescope, Lowell Observatory, optical, near infrared, telescope systems performance, commissioning, early science

1. INTRODUCTION

The Discovery Channel Telescope has been under active development since 2005 and since early 2013 has been engaged in regular science operations. Progress between the time of groundbreaking and 2012, the early phase of telescope commissioning, has been reported previously.[12345]

The DCT is designed to be a general purpose research telescope to accommodate the diverse needs of Lowell Observatory and its institutional partners. As such, it is a particularly versatile telescope, with provisions for substantial instrumentation at the prime, Cassegrain, Nasmyth, and bent-Cassegrain focal stations, relatively wide fields-of-view, and delivering seeing limited images over broad spectral bandpasses.

The telescope complex, located approximately 40 miles south-southeast of Flagstaff, is sited on National Forest Service land at an elevation of 2347m (7700 ft). It comprises a telescope enclosure, an auxiliary building housing the 4.3m coating chamber, a shop building within the nearby ranger station, and an astronomer's lodge. The telescope includes provisions for future upgrades, including a wide-field prime focus camera, and potentially very large instruments at the Nasmyth focii.

The system performance capability has been described in detail in previous papers [6789]. To date, most data gathered have utilized the Large Monolithic Imager (LMI) mounted at the Cassegrain straight-through port on the Instrument Cube, although some work using the Portable Occultation, Eclipse, and Transit System (POETS) and the Differential Speckle Survey Instrument (DSSI) has also been conducted. Integration of spectrographs is expected in the coming year.

In the last two years, the project has moved steadily into increased science operations. The percentage of time allocated to science observing in 2014 is expected to be slightly over 50%, with the DCT moving into full science operations starting in early 2015.

[a] L-3 Communications Integrated Optical Systems, Wilmington, MA
[b] All authors affiliated with Lowell Observatory, Flagstaff, AZ except as noted.

2. SYSTEM STATUS

Science operations began officially in January 2013. Time during 2013 and 2014 has been divided between commissioning work and science observations. The percentage of time allocated to science has been steadily increasing during that time, following roughly the trend we were aiming for (see Table 1). Most of the science observations done so far have been imaging, with a small amount of speckle imaging. Projects have ranged from the rotation period of comet Tempel2[10], to searches for and characterization of Kuiper Belt Objects, to studies of young stellar objects, very low mass stars, exoplanet transits, and weak lensing in galaxy clusters.

Table 1: Science Time Scheduled

Scheduling Quarter	Percent of available time scheduled for Science	Notes
2013 Q1	21%	
2013 Q2	23%	
2013Q3	24%	28 days subtracted for planned summer maintenance.
2013Q4	35%	
2014Q1	53%	
2014Q2	(56%)	Quarter not yet completed.
2014Q3	(68%)	21 days subtracted for planned summer maintenance. Quarter not yet completed.

The following sections summarize the status of the major subsystems.

2.1 Facility and Dome

Dome operation has been largely trouble-free since commissioning began in 2010. Engineering efforts since then have included automation of the mezzanine vent doors and fans, installation and optimization of lighting for the calibration screen, and normal maintenance of the shutter and azimuth drive systems.

2.2 Optics

The optical configuration of the telescope has been previously described[6]. Early testing revealed ghost images and reflections that led to investigation of possible sources of stray light. Inspection of the components along the light path led us to focus on the area below the stovepipe baffle, inside the M1 cell. Photographs taken from the instrument cube straight-through port (Figure 1) show multiple reflective surfaces in this area. These features are associated with the M1 cell, the M1 inner aperture mask, and M1 lifting fixture. A short baffle was designed and built (Figure 2), which mounts inside the M1 cell and renders these features invisible to the detector. This baffle was installed in March, 2014. Further discussion of remaining stray light investigation is provided in section 4.

The condition of the optics has been monitored periodically to support scheduling of re-aluminization. Before and after each CO2 snow cleaning, the reflectivity is measured using a Konica Minolta CM-700d spectrophotometer. This normally takes place on a monthly basis; at times the humidity level precludes snow cleaning and reflectivity measurements are not taken.

Figure 3 shows a summary of data from early 2013 through the present. As expected, there has been a significant drop in reflectivity on M1. Closer examination of the data shows that the specular component – excluded (SCE) measurement, generally taken to indicate the degree of scattered light, has increased markedly over the past year. The change in SCE is roughly 2/3 to 3/4 of the total reduction in specular component – included (SCI) measurement. We take this as an indication that the mirror is more in need of aqueous washing rather than wholesale re-aluminization. We plan to do this aqueous wash during the summer monsoon period this coming July.

The M2 reflectance data, not surprisingly, does not show the same evidence of degradation. The reflectance curves are much more tightly grouped compared to M1, and the trend of SCE over time is essentially flat. This result is consistent with the primarily downward-facing aspect of M2. M2 was also aluminized more recently than M1.

2.3 Mount

The mount has performed extremely well since it was commissioned, providing excellent blind pointing and tracking performance. The stability of the system is demonstrated by the very infrequent need to modify the pointing model. See section 4 for a discussion of the pointing and tracking performance.

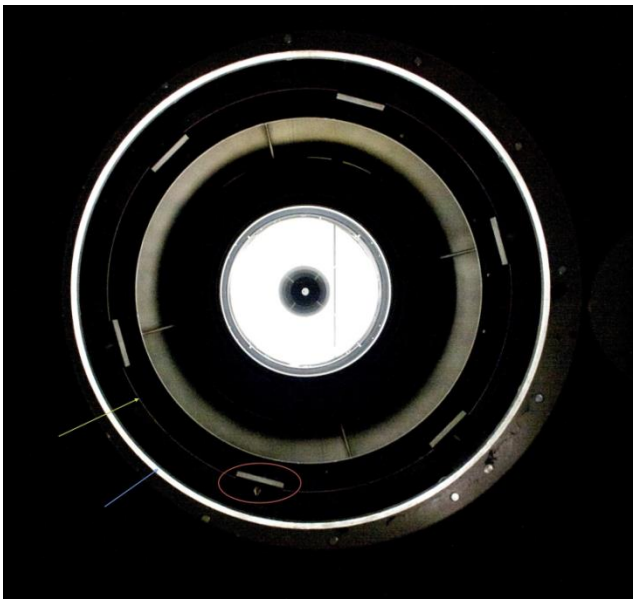

Figure 1 View at Instrument Cube prior to M1 Cell Baffle Installation. The outermost ring is the edge of one of the main bulkheads of the M1 cell. The set of six equally spaced rectangles are the ends of the lifting tabs on the lifting fixture. The diffuse ring inside that is the bottom portion of the stove pipe baffle.

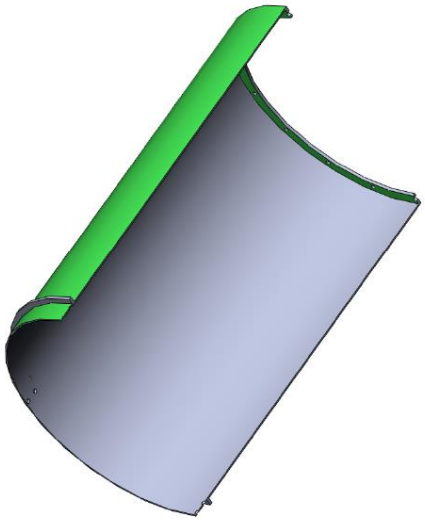

Figure 2 M1 Cell Baffle Design

In 2012, we discovered a glycol coolant leak in elevation motor #1. The elevation motors are frameless, direct-drive brushless DC motors. The stator of each motor (one in each yoke arm) is actively cooled by the facility propylene glycol-water system. The coolant circulates in circumferential passages in the stator which are enclosed by a coolant jacket. When the leak was discovered, investigation revealed evidence of corrosion in the coolant passages. The nature of the corrosion led to the conclusion that a galvanic couple between the stator housing and the coolant jacket, or some other wetted metal component, was the cause. To mitigate the corrosion, the coolant jackets of both motors were removed and treated with a polymeric coating which eliminates the potential for a galvanic couple. Sacrificial anodes were also added to the coolant circuit very close to the motor stators as a further precaution.

During the removal of elevation motor #1, we discovered damage to the potting compound which encapsulates the stator windings. The damage comprised cracks and blisters in the potting, Figure 4. The damage raised suspicions that the motor electrical integrity might have been compromised. Later testing showed that indeed the stator winding insulation resistance, which should be greater than 500 Mohms, measured 0.53 Mohms. After reviewing the test results, the motor manufacturer concluded that the motor life had been severely compromised and that it could fail completely at any time. Motor #2 was also tested and found to have acceptable insulation resistance.

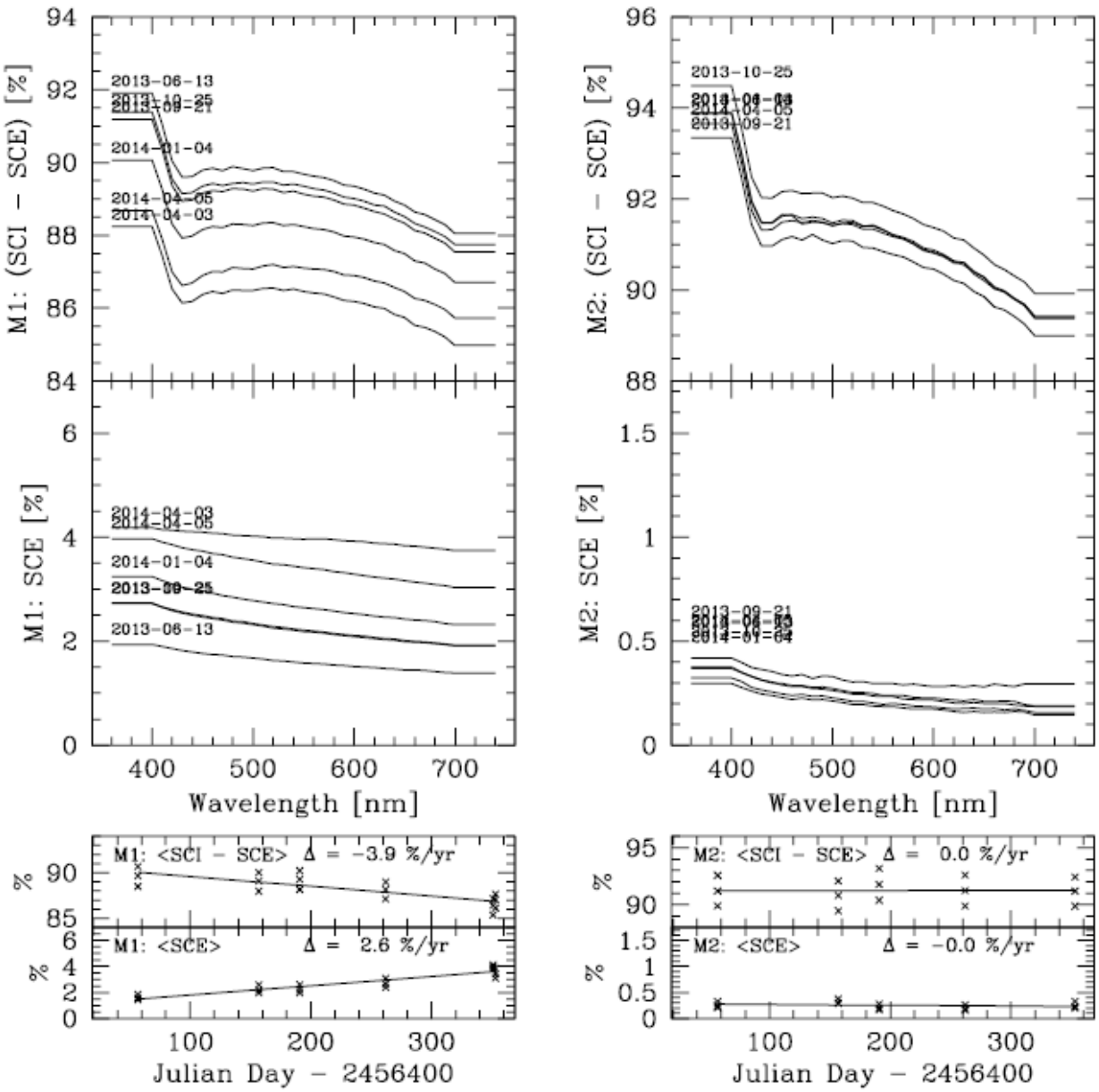

Figure 3 Results of Mirror Reflectance Measurements. Left column is for M1, Right column is for M2. The upper most panels show the mean of the specular reflectance (SCI-SCE) measurements as a function of wavelength for each date they were measured. The middle panel shows the nominal scattered light component (SCE) as a function of wavelength. The bottom two panels show the mean values, averaged over wavelength plotted against Julian day. We have fit for the change in <SCI-SCE> and <SCE> as a function of time. M2 shows essentially no change. M1 shows an increase in SCE of about 2.6% per year, and a decrease in (SCI-SCE) of roughly 3.9% per year.

Efforts began immediately to procure a replacement motor. This motor was received in March of 2014 and installed the following month, Figure 5. Post-installation testing has shown the new motor is performing well, and insulation resistance is excellent. We intend to measure the insulation resistance of both motors periodically, and will continuously monitor the temperature going forward in order to prevent similar failures.

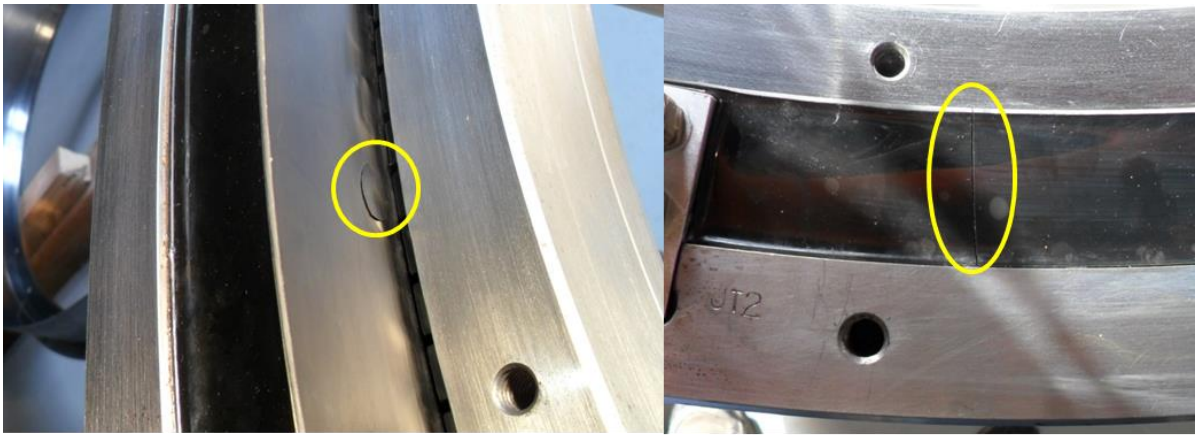

Figure 4 Damaged Elevation Motor Potting Compound

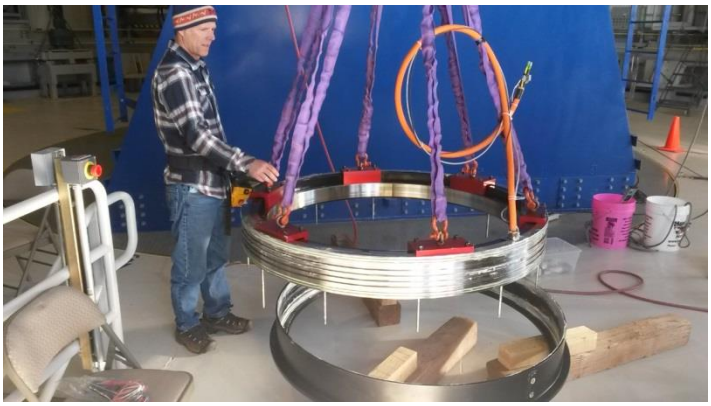

Figure 5 Assembly of Replacement Elevation Motor into Cooling Jacket

A root cause for the insulation resistance failure was not established. The cracking and blistering of the potting compound was unrelated to the corrosion issue with the stator housing coolant passages; it so happened that it was discovered at the time we investigated the coolant leak. The potting damage was possibly the result of overheating, though elevation motors #1 and #2 saw identical loads and operational conditions during commissioning, and only motor #1 showed the distressed potting compound. The elevation motors were tested during factory integration at GDST, and again during site acceptance testing, however such testing did not include measurements of insulation resistance. Since the motor continued to generate acceptable torque even with degraded winding insulation, it is difficult to pinpoint where in the integration cycle the damage occurred.

In the process of addressing the insulation resistance problem with elevation motor #1, the motor manufacturer notified us that they intended to cease production of this motor configuration in 2014. To support the facility long-term, we ordered another motor prior to end of production. This unit, to be delivered by third quarter 2014, will be our long-term spare in the event of another motor failure.

2.4 Active Optics System (AOS)

The design of the AOS has been addressed in detail in previous papers[6,7] and early image quality results described in 2012[5]. Results of recent testing are presented in section 4 below. From an operational standpoint, the subsystems comprising the AOS have been extremely reliable and remarkably trouble-free. In particular, the custom-built components of the primary and secondary mirror support systems have shown an impressively high level of reliability. To date, we have experienced one hardware failure, a stepper motor drive module for one of the 120 primary mirror axial support actuators. The drive in question was replaced and the system restored to normal operation with no impact to nighttime operations.

In the long run, we expect to have both an open-loop predictive model of the optical aberrations, as well as a closed loop wave front sensing system that will correct the residual aberrations. The main thrust of engineering testing since 2012 has been to determine the behavior of the low order optical aberrations as a function of mount temperature and zenith distance. The aim has been to construct the open-loop model, allowing us to predict the magnitude of the aberrations even when we are not able to do closed loop wave front sensing. After 18 months of data collection, we had enough data to populate the open-loop look-up table (in reality a set of coefficients we call the Wavefront Open Loop Model or "WOLM"). Table 2 below summarizes the current values of the WOLM.

Table 2 Current WOLM Coefficients

Measured Zernike[a]	Collimation or Bending Mode	Intercept	kZs	kZc	kMT	Correction is applied to:
			µm RMS/deg	µm RMS/deg	µm RMS/°C	
Z4 (Focus)	Z4	8.1176	0.2650	4.7680	0.6454	M2
Z7 (Y-coma)	Z7	0.0333	0.2609	0.2330	0.0196	M2
Z8 (X-coma)	Z8	-0.1257	0.2306	-0.1417	-0.0197	M2
Z5 (X-ast)	BM 0	-0.2097	-0.4605	0.1792	-0.0171	M1
Z6 (Y-ast)	BM 1	-0.3154	-1.1685	-0.1506	-0.0184	M1
Z9 (X-tref)	BM 3	-0.0540	-0.0157	-0.0011	-0.0028	M1
Z10 (Y-tref)	BM 4	-0.0176	0.1543	-0.2112	-0.0072	M1
Z11 (Spherical)	BM 13	0	0	0	0	M1

[a]Zernike term indexing follows the convention of Noll[11].

Table 2 represents the default corrections made to the optical system in the absence of any additional wavefront solutions input by the telescope operator. Each row of this table provides the coefficients for the equation which establishes the AOS correction delivered to the mirror supports subsystems for that Zernike or bending mode. For example, the correction for focus (Z4) is calculated as follows:

Open-loop focus correction = 8.1176 + 0.265 sin(Z) + 4.768 [1-cos(Z)] + 0.6454 (MT) µm RMS Z4

Where Z = zenith angle, radians
MT = mount temperature, degrees C

Note the absence of values for BM 13. BM 13 was found to be a much better match to spherical aberration than BM2[9]. Similarly, bending modes 5 and 6 are nulled in favor of using bending modes 16 and 17[9]. The coefficients in Table 2 have resulted in excellent open-loop image quality, for which performance is shown in section 4 of this paper. While the spherical term is not corrected by the WOLM, we do solve and correct for it when doing wavefront solutions.

2.5 LMI

The Large Monolithic Imager (LMI, Figure 6) is the DCT's optical camera. It uses a single large device rather than a mosaic of CCDs in order to avoid the ills associated with gaps between chips. This enables, for example, studies of galaxies down to extremely faint surface brightness, without the difficulties that come with changing sky levels while dithering to fill in the gaps. The use of a single CCD provides many additional advantages, such as the greater uniformity of color-terms than one typically finds from chip-to-chip. It also results in more efficient observing and ease of reductions.

At present, LMI is the only facility instrument on the DCT; we anticipate it will remain a principal workhorse instrument for many years. We anticipate that some of the near infrared instruments, like the near infrared spectrograph NIHTS, will use a dichroic pick-off mirror allowing simultaneous optical imaging with LMI.

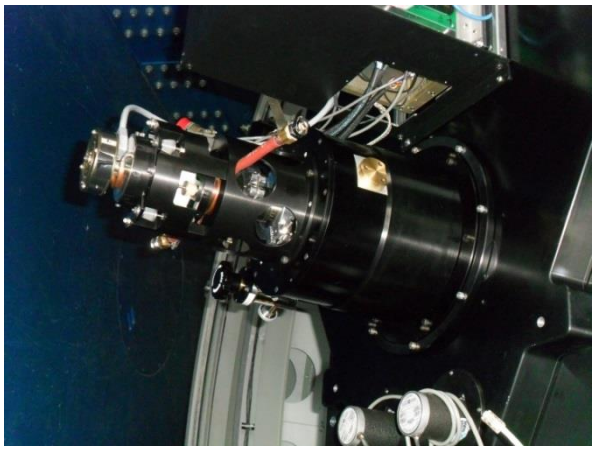

Figure 6 LMI During Installation, Sept 2012

Description of the Instrument

The imager is built around the first of e2v's 6144x6160 pixel CCD231-C6 devices. These 93mm square CCDs are the largest that fit onto a 150mm wafer. The CCD is nearly perfect cosmetically, a testament to the quality of the manufacturing processes in use at e2v. The 15-micron pixels oversample the point-spread-function at our focal plane, with a 0.12 arc-sec scale. The chip is usually binned 2x2 except for certain astrometric and photometric applications. The field of view is 12.3 arc-minute on a side. The CCD is cooled to -120 C using a Sunpower Stirling cycle cooler, resulting in negligible dark current.

The CCD is a deep depletion device and has a 4-layer AR coating, providing both high sensitivity from the near-UV through the red and extremely low fringing at long wavelengths. The measured quantum efficiencies are 43% at 350 nm, 90% at 400nm, 97% at 500nm, 93% at 650nm, and 59% at 900nm. There is a significant "quilted" pattern to the flat-fields at shorter wavelengths, a consequence of the annealing process used by e2v. The pattern amounts to about 9% (peak to trough) at U, 2% at B, and sub-one-percent at V, and flat-fields out very well.

Our 125-mm Bonn shutter allows very short exposure times (<0.1 sec) with good uniformity. The camera has a dual filter wheel that can accommodate up to 18 filters, each 4.75" square plus an open position.

Using an ARC (Leach) Gen III controller, we can read out the entire chip through a single amplifier in about 24 sec when binned 2x2; this time includes the pre- and post-scan. An unbinned frame takes 73 sec to read out through a single amplifier but about 20 sec if all four amplifiers are used.

The instrument is run using the Lowell Observatory Instrument System (LOIS), providing commonality with other Lowell telescopes as well as future DCT instrumentation. The astronomer interacts with the instrument and the control system using the Lowell Observatory User Interface (LOUI), a simple and intuitive user interface.

Challenges and Remaining Issues

One of the problems we became aware of early on was that there were significant residual images if some pixels were highly saturated. In quantitative terms, if the chip was exposed to 7.5 million electrons per pixel, about 50x saturation, the next image would show a residual image of about 90 electrons per pixel, fading down to the noise in about 10 minutes. Such residual images are a characteristic of deep depletion devices. To solve this, we implemented a clocking scheme in which the CCD is run in deep depletion mode when integrating and being read out, but in inverted mode, with lower clock level, when idling between exposures. This approach had been used successfully by Barrick et al. (2012) to eliminate the residual image problem in an e2v CCD42-90 deep depletion CCD used in a spectrograph on the Canada-France-Hawaii telescope[12]. In our case, we had to add a "transition mode" in switching between the inverted mode and deep depletion mode to keep the maximum clock swing within safe limits. This cured the problem with no negative effects. It also eliminated a problem we observed upon startup in which the bias levels were elevated, and required 10 minutes to return to operational norms. CCDs saturate when they are first powered on, and we were seeing the decay of the residual image from that "big bang."

The serial register clocking is also not yet optimal. There is some horizontal shading due to improper DC restore operation and there are streaks behind highly saturated images. The latter problem may be resolved along with the former one, but it may be unrelated. In this case it may be reduced with a slower readout rate or by using an unconventional anti-blooming scheme suggested by e2v to limit the amount of charge placed in the serial register. It should be possible to arrange the anti-blooming scheme so it is not detectable in normal use because the output node saturates at a significantly lower level than the full serial register pixel capacity, but it hasn't been tried and is not guaranteed to work.

Finally, we have yet to optimize the linearity. The departure from linearity is 3.5% over the range of 40 ADUs to 52,000 ADUs (120e- to 155,000 e-). The effect is only 1% from 20,000 to 52,000 ADUs (59,000 e- to 155,000 e-). To improve this, we will carry out repeated tests with different output gate and output drain voltages. In the meanwhile we have provided users with an approximate correction formula.

2.6 Controls and Software

In the transition from construction phase to commissioning and operations, the telescope software team faced a variety of software challenges, both foreseen and unforeseen, and addressed those with a variety of solutions including isolation of the control systems network, development of an Operations Log application, extension of the interface to instrumentation software, improvements to engineering data archival, provisions for fault tolerance, and enhanced user experience. This period has seen the successful development of a second phase of auxiliary features and applications that take advantage of the existing robust architecture to enhance the operation of the DCT. The next phase of development will entail work to further extend telescope automation capabilities and minimize ongoing maintenance required for software systems. A summary of the current state of the system software is provided separately in this conference[13].

2.7 Engineering and Operations Coordination

Night operations are currently supported by two full-time and three part-time telescope operators, with engineering and science staff available for phone support. For nine months, operators are scheduled on a two-shift-per-night basis with hand-over occurring at midnight. The remaining three months, from early May to early August, operators are scheduled on single shifts from dusk to dawn. The engineering crew typically works normal daytime hours, however they can be called in to support night operations as required.

3. COMMISSIONING RESULTS

3.1 Pointing and Tracking

We noted back in 2012[5], the pointing models for the mount were proving to be relatively simple, and the mount itself was generally well behaved. This behavior has continued. Figure 7 shows pointing data taken in May 2013 for construction of a pointing map. While the zero points for the azimuth and elevation axes have shifted, the basic structural behavior of the mount is the same as it was a year prior (see ref. 5). The pointing map in question is still in use as of early June 2014. At the beginning of each night of operation, we take a series of pointing checks. At the time the map was created, the typical dispersion of those collimation offsets was on the order of +/-3 to 5 arcseconds in each axis. The dispersion is still the same over a year later.

The pointing map currently consists of the six basic geometric terms (in TPOINT parlance IA, IE, NPAE, CA, AN, AW) and two flexure terms that are functions of elevation or zenith distance (PEE1, TX). We have looked at higher order terms and have (so far) not found them to be needed. Similarly, we have not needed to include terms for the offset of the instrument rotator axis, though we did investigate this in late 2012 and early 2013.

It is worth noting that the mean azimuth and elevation offsets can shift if the axis encoders are re-referenced. While not proven, the reason for this seems like to be a dependence upon which set of index marks on the encoder tape are used for referencing. In support of this, we find that if we reference starting at the same location, and moving in the same direction, the mean offsets tend to be very similar and close to zero. So, while the encoder tapes have absolute reference marks roughly every degree, operationally, we make a point of re-referencing at the same location. This is not something we need to do very often.

Since the tracking depends explicitly on the pointing map, with the map working well, it should come as little surprise that the tracking is generally good. The nominal drift rate has typically been on the order of 0.1 to 0.3 arcseconds per 5 to 10 minutes. Since the primary instrument in use now has a 12.3 x 12.3 arcminute field, and we have a working autoguider, there has been little need to improve this now. In the near future, when we bring near infrared and spectral instruments on-line, we expect that we will need to put more effort into improving the pointing residuals. Given our experience over the past 3 years, we don't expect this to be a major effort.

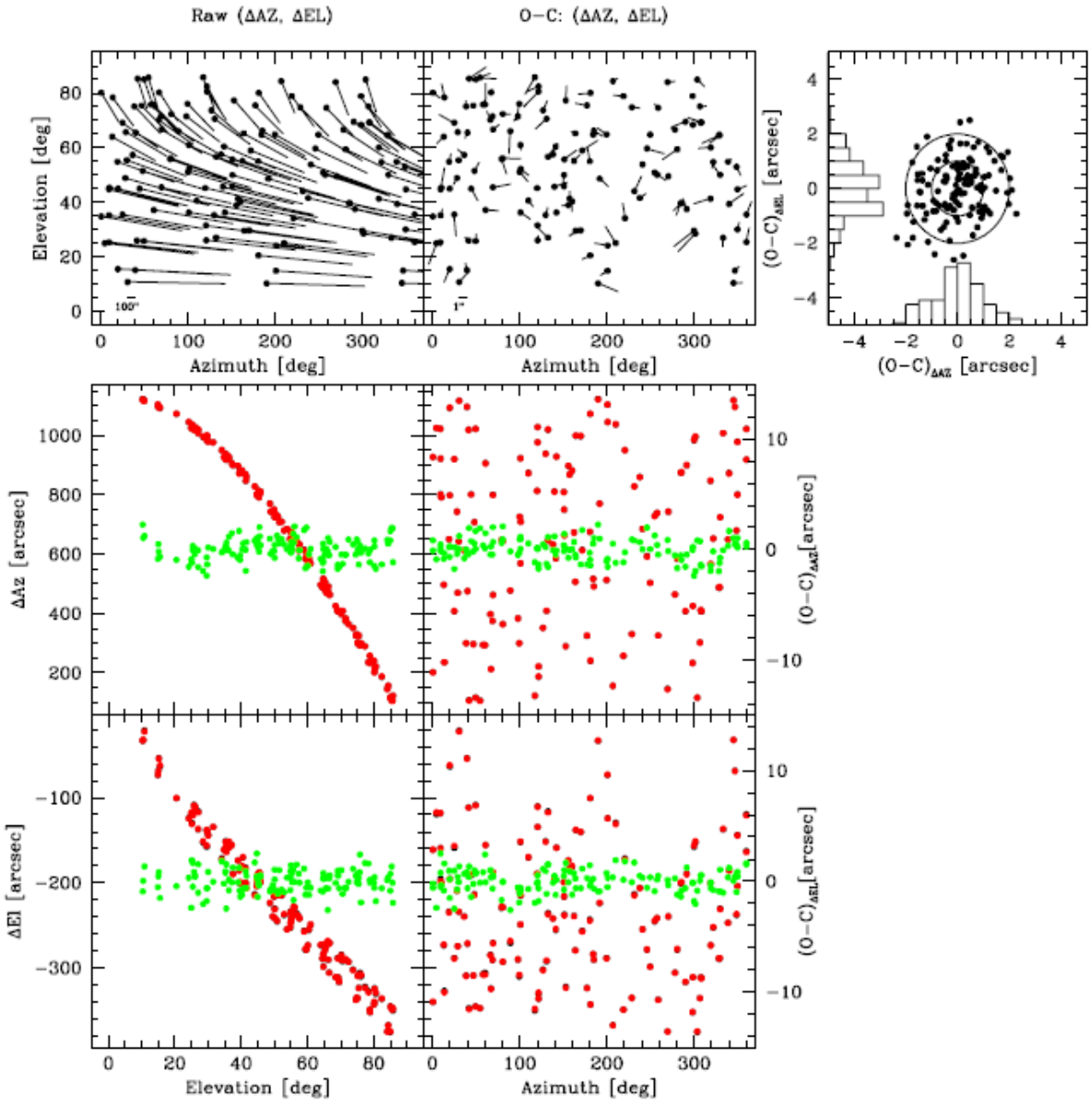

Figure 7: Pointing model data, taken in May 2013. Upper Left: The differences between the raw encoded azimuth and elevation, and the requested values. Upper Middle: The differences between the requested and actual, after correcting for the pointing model. Upper Right: Residuals in the pointing model fit. The concentric circles are 1 and 2 arcseconds in radius. The Lower 2x2 plots show the differences between the requested and encoded azimuth and elevation as functions of azimuth and elevation. The points in the black (mostly hidden) are the original differences, those in red are the differences predicted by the fitted pointing model, and the green points are the final Observed minus Calculated (O-C) residuals in arcseconds (axis limits on the right side).

Because a large fraction of the Lowell staff observe solar system objects, the TCS was required to implement non-sidereal and ephemeris based tracking. Both of these have been tested and work nicely. Figure 8 shows sidereal and non-sidereally tracked images of the field of two main belt asteroids. Both are 300 second, unguided exposures, and each shows FWHM of the tracked objects of between 0.7 and 0.8arcseconds.

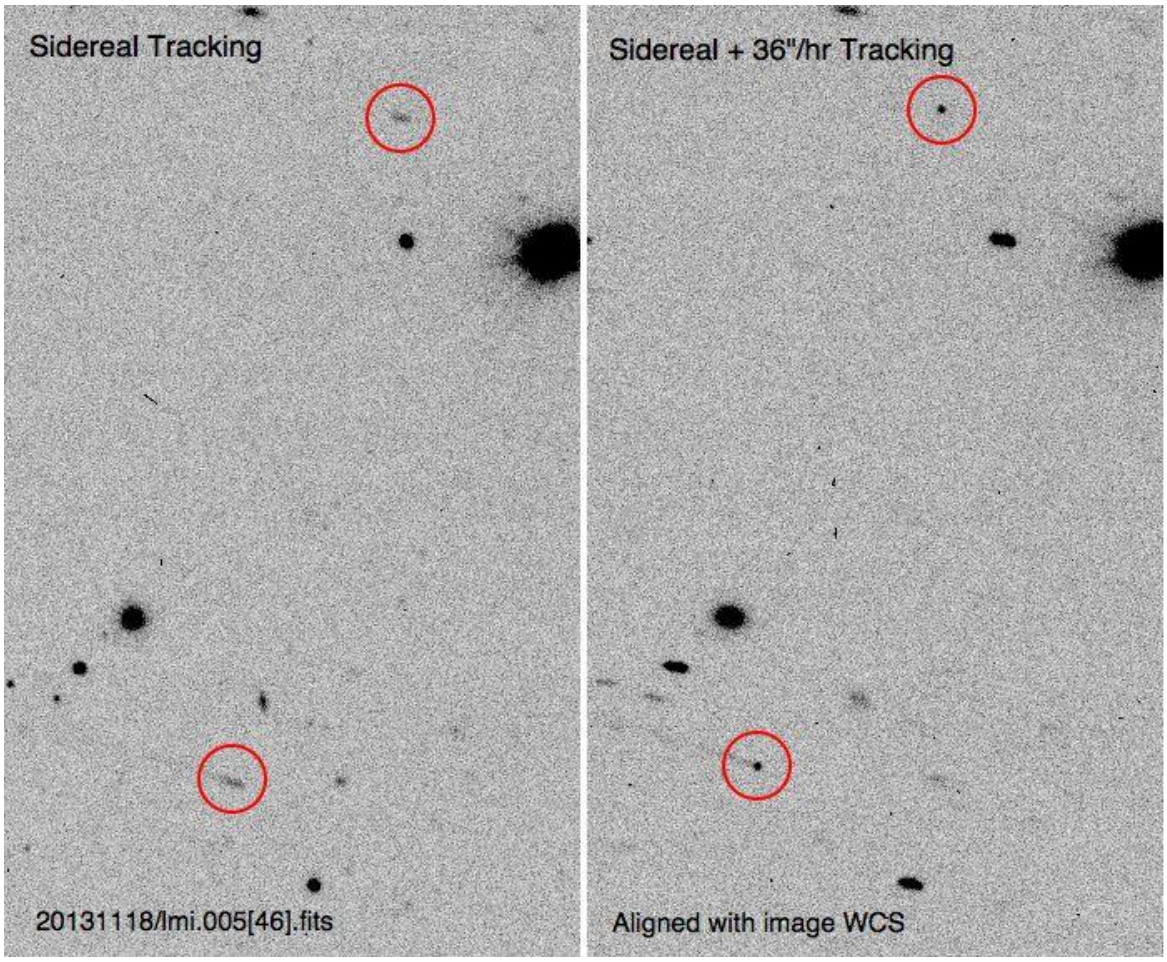

Figure 8: Two unguided, 300 second exposures of the field of two main belt asteroids. The left panel shows the image taken while tracking at sidereal rates. The right panel shows the same field when tracking at sidereal plus 36"/hr. The objects circled in red are both main belt asteroids. In the left image, the FWHM of the stars is between 0.7 and 0.8". In the right image, the FWHM of the asteroids is between 0.7 and 0.8".

As noted above in section 3.3, one of the two elevation motors was considered suspect. To understand the impact on the pointing and tracking if the motor should fail, we tried the experiment of tracking with both motors and with only one. While not the desired way to operate, we found that we could continue to operate within acceptable limits, though with slightly degraded performance on only on elevation motor (see Figure 9). The test was done for over 8 minutes in two and one motor mode each, with guiding off (so as to avoid measuring the guided corrections). The RMS residual jitter (after de-trending) when running with two and one motors is 0.1" and 0.13" respectively. These are both well within acceptable limits, given typical site seeing between 0.7 and 1.0", and even under good conditions of 0.5" they are workable. We did not do the experiment with the guider running, but expect the results to be at least as good.

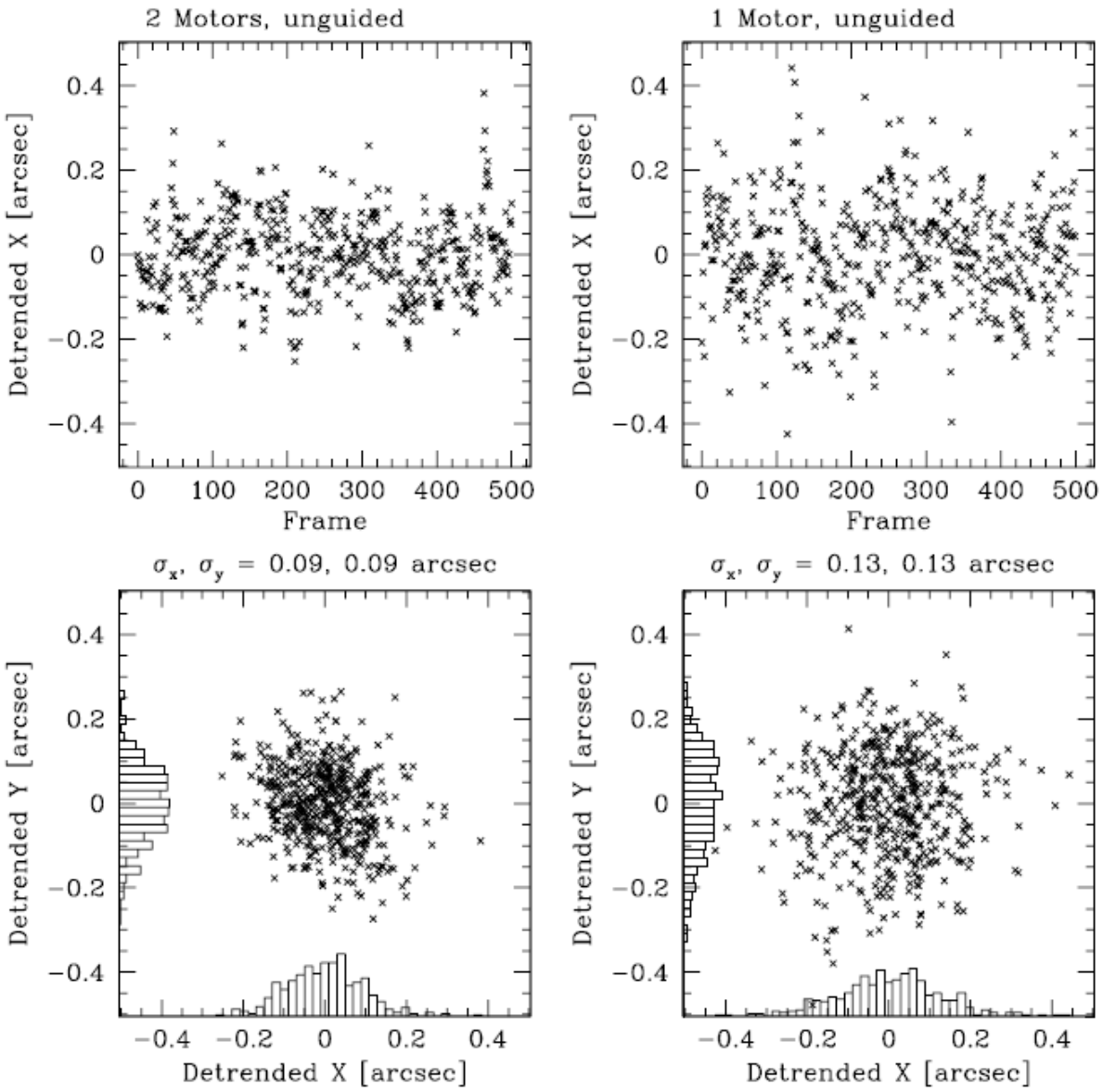

Figure 9: Two (left column) and one (right column) elevation motor performance. The upper panels show the de-trended jitter in the x centroid of a single star on the optical axis versus time (frames were taken once a second, so the time span is a little over 8 minutes). The lower panels show the x vs. y centroids for the same data set, after removing the slow drift term from pointing model residuals. The RMS scatter with two motors is just under 0.1", with one motor it increases to 0.13", still within acceptable limits.

3.2 Guiding

As part of the instrument cube, there are two probes which can serve as guiders or wavefront sensors. Guiding is working and can be done from either probe. The guider is used primarily to correct for the slow drift of the pointing map. The guider normally operates on a 1Hz cadence, and can use stars down to about 14th magnitude at that rate. Given the very slow nature of the drift, we can slow down the guiding and go 1.5 to 2 magnitudes fainter if need be. The guide probes are equipped with a UBVRI set of filters to help match the operating wavelength of the instruments. The TCS is capable of computing and correcting for the differential color refraction if the guider is operating in a significantly different bandpass than the science instrument.

3.3 Delivered Image Quality

In additional to good seeing, one of the critical aspects of the image quality is the degree to which the stellar PSF is constant (or varies) across the focal plane. In an effort to assess this, and the astrometric field distortion, we took a series of images of the well-studied open cluster M67. The images were taken a range of rotation angles and linear offsets. The night in question had typical seeing around 1.2". We used the 2-D Gaussian PSF model in SExtractor[14] to measure the FWHM, ellipticity (1-b/a) and orientation of all the sources within the images. The detection lists were cross-matched with the UCAC2 astrometric catalog[15] and only those objects that matched stars were retained. In addition, we also removed all objects that had any SExtractor internal flags set (those indicating possible contaminated, blended, or saturated objects). In Figure 10 we plot the distribution of the FWHM and ellipticity of this full sample of clean stellar PSFs. The left hand column shows the histograms of the overall distribution of values; the right hand column show the mean values of these measures within annular bins in radius; the error bars are one sigma errors. Only bins with at least 30 objects have mean and sigmas plotted. What we see is that in both FWHM and ellipticity, the stellar PSFs are very uniform across the field, as would be hoped.

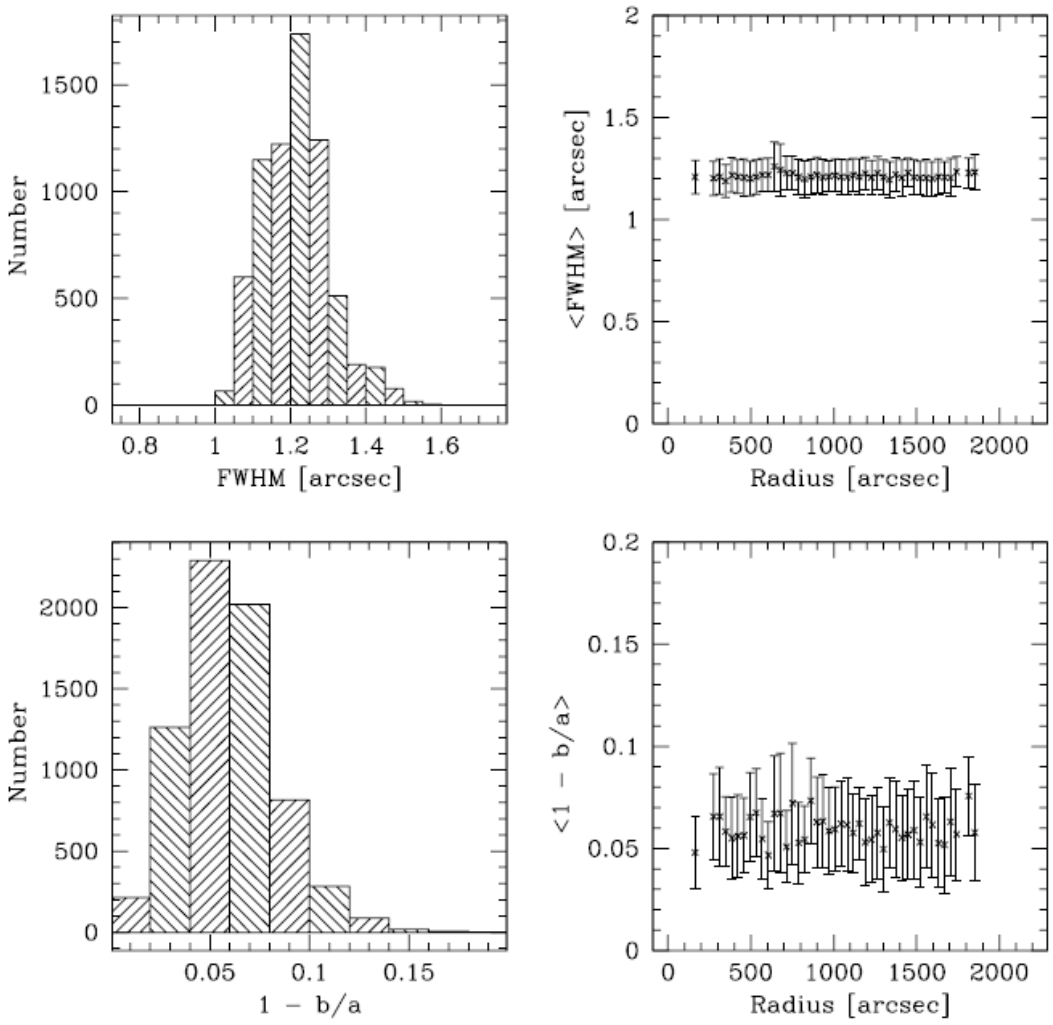

Figure 10: Constancy of the stellar PSF across the field of view of LMI. The upper panels show the FWHM across the field, the lower two the measured ellipticity (1-b/a). The left hand column show histograms of the distribution of individual measures of the FWHM and ellipticity. The right hand column shows the mean values of the FWHM and ellipticity in annular bins of increasing radius from the optical axis. Only bins with more than 30 stars were used. The plotted error bars are the one sigma RMS.

The seeing at the DCT has been as good as slightly better than 0.5", and is often between 0.7 and 0.9". At the moment we do not have comprehensive statistics on the site seeing to compare with those measured during site testing[16]. Based on anecdotal evidence, we do appear to be getting seeing in line with the site measurements, and consistent with the Delivered Image Quality budget put together early in the project history.

3.4 Astrometric Performance

Using the same M67 cluster data, we also looked at the astrometric performance of the system. The set of data includes sets of 5 images at each of 21 position angles. The plate scale determined from the linear plate solutions was consistently 0.240"/pixel (binned 2x2) in both x and y at all rotation angles. The CCD column and row directions were within +/- 0.005degree of perpendicular. The mean RMS for the linear plate solutions against UCAC2 were 99 and 87 milli-arcseconds in ζ and η respectively over an average of 134 reference stars in the field.

We also created a preliminary map of the field distortion pattern (FDP) (see Figure 11) from the ensemble of astrometric linear and 3rd order plate solutions of M67. We combined all the matched star residuals within a 16x16 grid of bins. Within each bin that had at least 10 detections, we computed the mean residual. Those bins with fewer are not plotted. The most prominent term is the 3rd order radial term, which can be seen in the CCD corners, and to a lesser degree near the center. For comparison, the right panel of Figure 11 shows the residual FDP after a 3rd order solution.

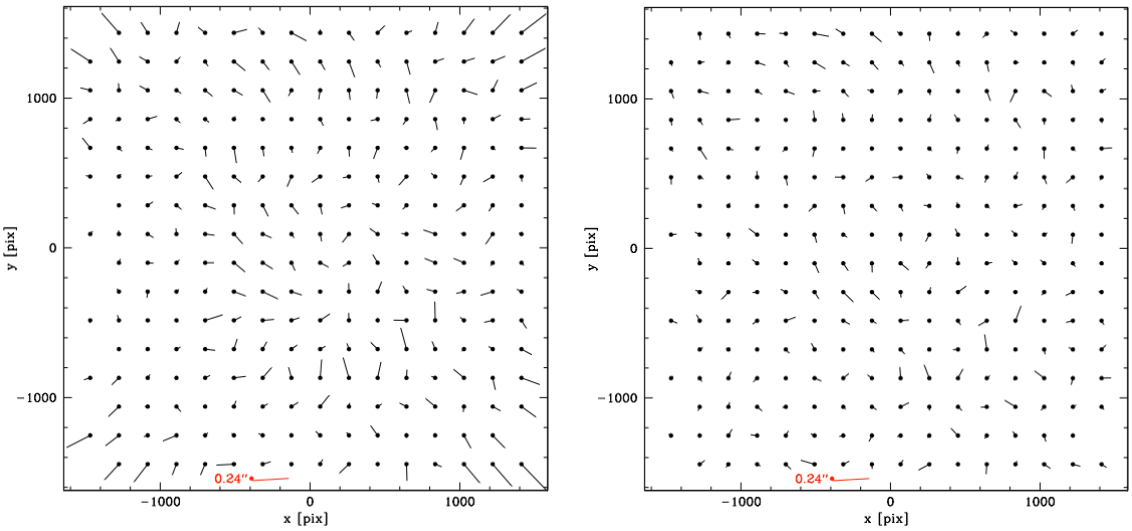

Figure 11: Residual astrometric field distortion pattern, after a full linear (left) and 3rd order (right) plate solution. For scale, the red line at the bottom indicates the size of a binned 2x2 LMI pixel (0.24"). The most prominent features on the left are the 3rd order radial term, which shows most clearly in the corners, and a little bit in towards the center; they are taken out nicely on the right.

4. REMAINING COMMISSIONING TASKS

Commissioning of the telescope systems is largely complete. A few engineering tasks remain, described below. The focus of development effort over the next year is to complete the development of and commission the spectrographs planned for DCT: the Near-Infrared High Throughput Spectrograph (NIHTS) and the DeVeny Spectrograph. Discussion of the progress on their development is provided in a separate paper[17].

4.1 Calibration screen illumination system

At the DCT, we have mounted a large projection screen painted with Labsphere 6080 white reflectance paint. This materially is optically stable, and has very high reflectance (95-98%) from 300 to 1200 nm. The screen is currently illuminated on three sides using 12-volt DC lamps on booms. (The central lower boom is retractable to avoid interference as the dome rotates.) The calibration system is carefully voltage regulated, and tests show that after an initial warm-up period of ten minutes or so, the illumination is stable to a small fraction of a percent.

One of the challenges with the illumination system is that the distance from the top end of the telescope to the projection screen is only 7 feet; this poses significant problems for obtaining uniform illumination from the top end. On the other hand, illuminating the screen from the side results in only scattered light reaching the primary mirror, a very different situation then when the telescope is illuminated from the sky.

For use with LMI, we find that large-scale bright twilight flats match the dark night sky to about 0.5% or better. Dome flats obtained with our calibration screen are more convenient, but match the dark night sky to only 3-4%. We are currently investigating to see if we can do better by illuminating the spot from the top ring, and looking at other ways we can improve the uniformity from the sides.

4.2 Wind shake characterization

Another commissioning task remaining is the careful study of windshake data, to define strategies to optimize performance as a function of wind speed and direction. Recent telescope operation (spring of 2014) has resulted in certain ad hoc tactics being implemented by the telescope operators; for example closing ventilation doors on the upwind side of the dome, or closing odd-numbered doors on all sides of the dome. While these actions may indeed reduce the impact of wind on the telescope performance, their effectiveness has not been systematically evaluated. The ventilation door design was envisioned to permit modulation of the openings depending on wind speed and direction, with a door motion increment of perhaps 25%. Significant data on windshake at various speeds and directions is necessary to design the control system.

4.3 Stray light characterization

In addition to the baffling of the inside of the M1 cell, we have tracked down several additional sources of scattered light within the instrument cube. Temporary baffles have been installed demonstrating that we have properly identified the surfaces, and we are in the process of fabricating permanent baffles, which will be installed this summer. As an example Figure 12 shows the effect of baffling the lens cell for the upper element of the RC corrector; at a radius of about 27arcmin, a bright source was catching the metal surface of the cell (left panel). Two additional surfaces within the instrument cube have also been identified and remediated in the same manner. The scattered light performance has improved dramatically.

4.4 Closure of Wavefront System with Active Optics System

The Active Optics System was designed to support automated sensing, solution, and correction of up to 47 Zernike terms. The closure of this control loop is an outstanding task that has frankly not been addressed because of the remarkable stability of the optical system. We find that performing a wavefront solution, and applying the resulting corrections once or twice per night is adequate for our user's current needs. However, in anticipation of more critical needs, especially as regards the imminent commissioning of our spectrographs, we intend to "close the loop" with the wavefront sensor. This will require two main things. First is development of code to automate the wavefront solution, and second is to map out the dependence of the aberration terms on radial distance from the optical axis. The AOS software is ready to support this integration, however adjustments to various gains will likely also be required.

4.5 Non-Sidereal Guiding

To support both moving object work, near infrared and spectroscopic observations, we are working to implement guiding that works with telescope motions that are not sidereal. This will include guiding (a) at simple non-sidereal rates (b) with an ephemeris tracked target and (c) while doing small, discrete motions of the telescope (like dithering on a field). All these modes depend upon a good understanding of how the guider stages move and how those and the CCDs are oriented with respect to the sky. Much of the work has already been done, and we expect to finish this up by the time the first near infrared instruments show up later this year.

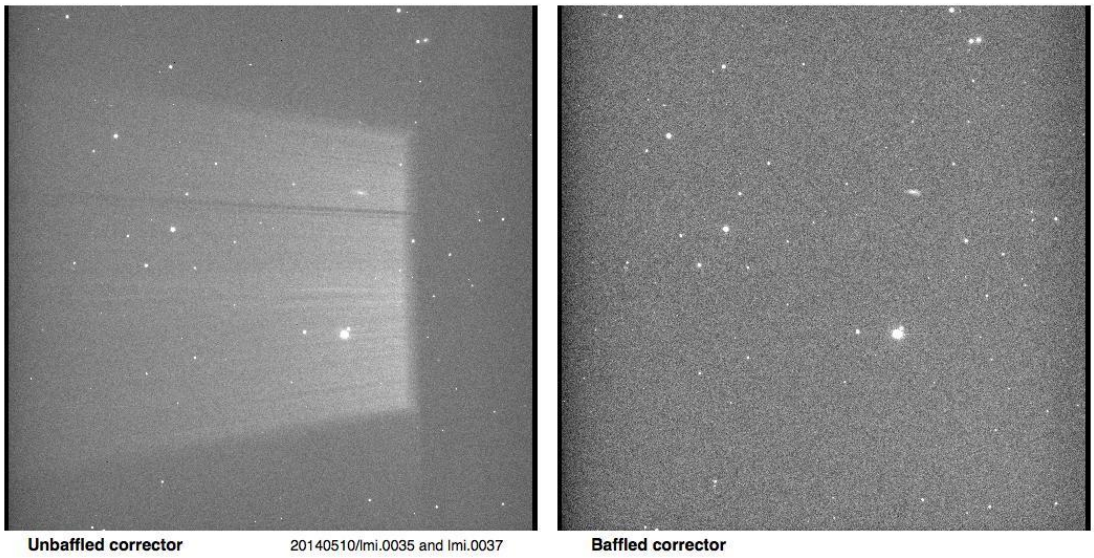

Figure 12: Effects of baffling the RC corrector upper lens cell. The left panel shows the impact of a light from a bright star 27 arcminutes off the optical axis reflecting of the corrector cell. The right panel shows the same field after installation of a temporary baffle.

5. LESSONS LEARNED

5.1 Spares

The construction budget for DCT made no explicit allowance for purchasing spare hardware. During the procurement of batch piece parts (such as for AOS actuators), we attempted whenever possible to buy a small number of spare parts, but the result was the ability to assemble at most one spare actuator. In other areas, such as dome mechanisms, we acquired spares of some inexpensive items such bearings or rollers, but not more expensive items such as gearboxes, couplings, and rack and pinion assemblies. In some areas, such as the mount, no spares were acquired whatsoever. This left us in the precarious position that in the event of a hardware failure, we would suffer downtime equivalent to the full procurement lead time for many critical subsystem components. The near-failure of the mount elevation motor, described in section 3, was a good example of such a brush with disaster. In that case, we were fortunate in two respects: the defective motor was capable of adequate torque for normal operation; and the mount is capable of operating, although with degraded accuracy, on one motor (see section 3.1).

Recognizing this weakness, we have strived over the past three years to address this problem in a systematic manner. Each year we have budgeted for critical spare hardware, focusing initially on those items with the longest lead time. Since telescope commissioning began, we have acquired spares for critical items such as the mount azimuth gearbox, mount single-board computers, and various electronic boxes including the time server, rack-mounted computer, and certain sensors.

This effort continues as each fiscal year we drill down farther into the system parts lists and ferret out those items that ought to be spared. We recognize that ultimately, this approach is more costly than if the spares had been bought along with the original system procurement contracts, but we had little choice due to funding limitations at the time. The lesson for other projects: plan for spares at the beginning to minimize life-cycle cost, and reduce the risk of loss of science time due to failures in the future.

5.2 Electric Power Reliability

The DCT facility is located at the end of a power circuit which is approximately 40 miles long. The circuit is an above-ground power feeder that winds through miles of sparsely populated pine forest. As such, it is subject to frequent power

outages as a result of high winds, lightning strikes, and snow loads. Naturally the facility design took this into account, and provided a 64 kW/80 kVA uninterruptible power supply with a 180 kW/225 kVA back-up diesel generator to address the power failure scenarios. The back-up power system ensures uninterrupted operation of computers and allows graceful shutdown, but is not intended to allow continued observations. Generally, power outages at the site last only a few minutes, with the occasional outage lasting a few hours. In general, the system has worked well. However, in recent months two power failures resulted in problems that were not anticipated in the original design.

The first failure regards the operation of the diesel generator itself. On August 19, 2013, a power outage was experienced that lasted several hours. The UPS provides automated e-mail and text alerts that indicate a power transfer has taken place. However, the diesel generator controls provide no such alerts. On the occasion in question, the diesel generator failed to start, and since the site was unmanned at the time, this resulted in exhaustion of the UPS and a complete power loss to the facility computers and equipment. Although no damage was done, the complete loss of power meant the loss of cooling for the LMI dewar, and a lengthy dry-out of the dewar window and re-start was required. Additionally, the facility UPS batteries were completely depleted, which is not a catastrophic failure but does reduce the battery life. Subsequent investigation showed the diesel engine starter battery had discharged due to a failure in the charging circuit.

The corrective action was to repair the charging circuit; in addition we took other steps to prevent a reoccurrence, or at very least to enable remote detection of such a problem. We now perform a routine test of the diesel generator once a month, including demonstration of power transfer, and we installed a webcam at the generator status panel to enable remote monitoring of operation in the event of a power outage.

The second power failure revealed a problem with the facility power distribution scheme. The facility compressed air supply is used, among other things, as a source of low-dewpoint air to prevent condensation on the LMI dewar window. Without the compressed air supply, the window frosts over quickly, the rate depending on the ambient humidity. Further, once frosted, restoration of the compressed air supply requires significant time to remove the frost through sublimation. In fact, the ratio of time required for sublimation to time allowed to frost up is roughly 1:1.

Until recently, the loss of electrical power meant loss of compressed air since the air compressor was not powered by the diesel generator; compressed air is not essential for a safe shutdown. Provided power outages are short, this was not an issue as we can tolerate brief losses of compressed air with little or no frosting of the LMI dewar window. On September 26, 2013, however, we experienced a power outage that lasted over 24 hours. Clearing the LMI dewar window after power was restored took a similar, and frustrating, length of time. The solution, implemented in May 2014, was to re-wire the air compressor to source the diesel generator power panel.

The third issue relates to the behavior of three-phase motors during certain types of power failures. Frequently, the power outages experienced at DCT have been a loss of a single phase. Although most of the telescope and dome motors are powered by servo amplifiers or variable frequency drives, several facility systems utilize induction motors powered directly by the mains. When a single phase is lost, this can mimic a phase reversal and cause the motor to operate backwards. In some cases, for example refrigerant compressors, backwards operation can result in permanent damage to the compressor. Further, we learned the hard way that many packaged system suppliers (such as chillers and pumps) do not provide electric power protection as a standard feature. Fortunately, power protection modules for such motors are relatively inexpensive, and we have installed such modules on all large motors. The modules detect specific power transients such as phase loss, phase rotation reversal, voltage sags, etc., and disconnect the motor load, reconnecting only when mains power parameters are stably within acceptable limits.

Summarizing the lessons learned in this area:

- Back-up power systems, even when new, must be periodically checked and confirmed operating normally. Undetected failures in seldom-used circuits or subsystems can render the back-up power useless when most needed.

- The supply of back-up power to facility equipment must be carefully considered. It is not enough to power only those computers and systems necessary for safe shut-down, rather all systems must be considered that could lead to damage or degraded operation upon re-start after a lengthy outage.

- The suppliers of systems powered by large 3-phase motors such as compressors, chillers, and pumps, do not by default provide power protection for their motors. Such protection should be specified during procurement or provision made for the addition of such protection upon installation.

5.3 Encoder Tape Cleanliness

The DCT telescope positioning is precisely controlled in 3 axes (azimuth, elevation, Cassegrain rotator) using angle encoders consisting of optical encoding tape and optical read-heads supplied by Heidenhain. As with any optical positioning system, cleanliness of the optical surfaces is important in order to maintain system accuracy.

Aggressively maintaining the tape cleanliness is vital. Even slight accumulations of dust, grease, or oil on the tapes can interfere with performance. Cleaning the tapes is a delicate process, because of the need to avoid scratching them, however cleaning the readheads is virtually impossible in-situ. The process involves removing the readheads, carefully cleaning the windows on each readhead, and replacing and re-aligning the readheads. Even with the recommended readhead alignment tool, this is a difficult and time-consuming task, with 6 readheads to align on the elevation axis alone. To mitigate the issue, we designed and implemented a system of vernier mounts to support rapid re-alignment of the elevation position readheads, which by virtue of their exposed location are most likely to be bumped or become contaminated.

5.4 Initial Check out of the Active Optics System

Because the secondary mirror was not finished at the time we installed the primary mirror, we constructed a small prime focus camera to use in checking out the primary mirror systems. This operational division of labor turned out to be a very good way to debug the primary mirror controls; the lack of the added complication of a second major optic in the system made it much simpler to track down sign, scale and orientation issues. In hindsight, had the secondary been ready when the primary was installed, because of the simplifications, it would still have been worth delaying installation of the secondary.

6. ACKNOWLEDGMENTS

These results made use of the Discovery Channel Telescope at Lowell Observatory. Lowell is a private, non-profit institution dedicated to astrophysical research and public appreciation of astronomy and operates the DCT in partnership with Boston University, the University of Maryland, the University of Toledo, and Northern Arizona University. LMI construction was supported by a grant AST-1005313 from the National Science Foundation. NIHTS is funded by a grant from NASA's Planetary Astronomy and Planetary Major Equipment programs. The upgrade of the DeVeny optical spectrograph has been funded by a generous grant from John and Ginger Giovale. The DCT is sited on land in the Coconino National Forest of the US Forest Service, and we are delighted to recognize their willingness to work with us.

Lowell Observatory owes a large debt of gratitude to the many engineers, scientists, contractors, and technicians who designed, built, and commissioned the DCT. An exhaustive list of these individuals would span many pages and is omitted here.

7. REFERENCES

[1] Sebring, T.A., Dunham, E., Millis, R.L, The Discovery Channel Telescope – A Wide Field Telescope in Northern Arizona, Proc. SPIE 5489-48 (2004)

[2] Smith, B.W., Bida, T.A., Millis, R.L., Dunham, E.W.,Wiecha, O.M., Marshall, H.K., Discovery Channel Telescope Progress and Status, Proc. SPIE 6267-05 (2006)

[3] Finley, D. T., Squires, C., McCreight, B.A., Smith, B.W., Chylek, T., Venetiou, A., Design of the Discovery Channel Telescope Mount, Proc. SPIE 7012, 70124I (2008)

[4] Smith, B., Chylek, T., DeGroff, B., Finley, D., Hall, J., Lotz, P., McCreight, B., Venetiou, A., The Discovery Channel Telescope: Early Integration, Proc. SPIE 7730, 77330A (2010)

[5] Levine, S. E., Bida, T.A., Chylek, T., Collins, P.L., DeGroff, W.T., Dunham, E.W., Lotz, P.J., Venetiou, A.J., Zoonemat Kermani, S., Status and Performance of the Discovery Channel Telescope During Commissioning, Proc. SPIE 8444, 844419 (2012)

[6] MacFarlane, M.J., Dunham, E.W., Optical Design of the Discovery Channel Telescope, Proc. SPIE 5489-65 (2004)

[7] Smith, B, Chylek, T., Cuerden, B., DeGroff, B., Lotz, P., Venetiou, A., The Active Optics System for the Discovery Channel Telescope, Proc. SPIE 7739-63 (2010)

[8] Smith, B., Manuel, A., Delivered Image Quality Budget for the Discovery Channel Telescope, Proc. SPIE 7738-4 (2010)

[9] Venetiou, A.J., Bida, T.A., Discovery Channel Telescope Active Optics System Early Integration and Test, Proc. SPIE 8444, 84441E (2012)

[10] Schleicher, D. G., Knight, M. M., Levine, S. E., The Nucleus of Comet 10P/Tempel 2 in 2013 and Consequences Regarding its Rotational State: Early Science from the Discovery Channel Telescope, AJ, 146, 137 (2014)

[11] Noll, R., Zernike polynomials and atmospheric turbulence, JOSA, 66, 207 (1976)

[12] Barrick, G. A., Ward, J., & Cuillandre, J-C., Persistence and Charge Diffusion in an E2V CCD42-90 Deep Depletion CCD, Proc. SPIE 8453, 84531K (2012)

[13] Lacasse, M., and Lotz, P. J. Discovery Channel Telescope software progress report: Addressing early commissioning and operations challenges, Proc. SPIE SPIE 9152-3 (2014)

[14] Bertin, E., Arnouts, S., SExtractor: Software for source extraction, A&Ap Supp., 117, 393 (1996)

[15] Zacharias, N., Urban, S. E., Zacharias, M. I., Wycoff, G. L., Hall,D. M., Monet, D. G., Rafferty, T. J., The Second US Naval Observatory CCD Astrograph Catalog (UCAC2), AJ, 127, 3043 (2004)

[16] Bida, T. A., Dunham, E. W., Bright, L. P, Corson, C., Site testing for the Discovery Channel Telescope, Proc. SPIE 5489, 196-206 (2004)

[17] Bida, T.A., Dunham, E. W., Massey, P.L., Roe, H. "First-generation instrumentation for the Discovery Channel Telescope", Proc. SPIE 9147-96 (2014)